ACS APPLIED MATERIALS & INTERFACES

Forum Article

www.acsami.org

Reduced Graphene Oxide-Supported Gold Nanostars for Improved SERS Sensing and Drug Delivery

Yusong Wang,[†] Lakshminarayana Polavarapu,[†] and Luis M. Liz-Marzán*[,†,‡]

[†]Bionanoplasmonics Laboratory, CIC biomaGUNE, 20009 Donostia-San Sebastián, Spain

[‡]Ikerbasque, Basque Foundation for Science, 48011 Bilbao, Spain

Supporting Information

ABSTRACT: Development of novel surface-enhanced Raman scattering (SERS) substrates and how they interface target analytes plays a pivotal role in determining the spectrum profile and SERS enhancement magnitude, as well as their applications. We present here the seed-mediated growth of reduced graphene oxide-gold nanostar (rGO-NS) nanocomposites and employ them as active SERS materials for anticancer drug (doxorubicin, DOX) loading and release. By this synthetic approach, both the morphology of rGO-NS nanohybrids and the corresponding optical properties can be precisely controlled, with no need of surfactant or polymer stabilizers. The developed rGO-NS nanohybrids show tunable optical properties by simply changing growth reaction parameters, improved stability as compared to bare Au nanostars, and sensitive SERS response toward aromatic organic molecules. Furthermore, SERS applications of rGO-NS to probe DOX loading and pH-dependent release are successfully demonstrated, showing promising potential for drug delivery and chemotherapy.

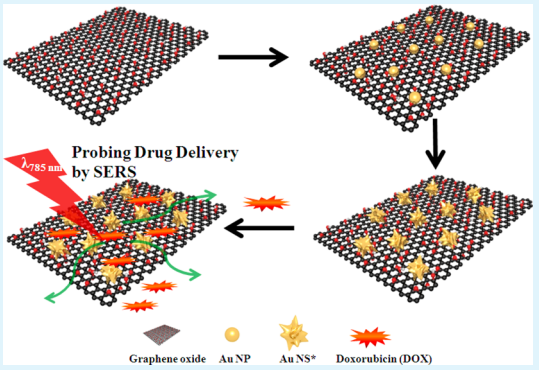

KEYWORDS: *reduced graphene oxide (rGO), gold nanostars, surface-enhanced Raman scattering, SERS, drug delivery*

1. INTRODUCTION

Surface-enhanced Raman scattering (SERS) has been widely applied in various fields, such as biosensors, environmental monitoring, and medical diagnostics and theranostics, because of its ability to provide molecular fingerprint spectra down to the single molecule level, through the enhancement of Raman scattering signals.[1,2] The development of novel SERS substrates and how they interface target analytes plays a pivotal role in determining the enhancement magnitude and spectrum profile of SERS.[3] One specific example is the ultrasensitive SERS detection that has been reported for Au nanostars supported on planar Au substrates.[4−6] Research by different groups on Au nanostars has pinpointed these nanostructures as excellent SERS substrates.[7,8] However, interfacing plasmonic noble metals with nonthiolated molecules is still a significant challenge because of the low affinity of such molecules to metals such as silver and gold and the short distance range of the SERS effect.[3,9] To overcome such problems, various strategies have been developed to trap and retain molecules for enhanced SERS.[8,10−13] For example, thermally responsive microgels have been used to encapsulate metal nanoparticles, so that the Raman active molecules could be trapped in the pores of the microgel, thereby reaching the metallic core and producing significant SERS signals.[10,11] Various other coatings such as silica shells,[12] bovine serum albumin,[8] and lipid bilayers,[13] have also been reported to trap the molecules close to metal nanoparticle surfaces.

Graphene and its derivatives (such as graphene oxide, GO, and reduced graphene oxide, rGO) have recently emerged as potential materials for various electronic and biological applications.[14,15] The unique structure of sp^2-carbon 2D nanosheets is favorable for aromatic molecule interaction via $\pi-\pi$ stacking and hydrophobic interactions between analytes and polyaromatic domains on the surface of graphene or its derivatives, and therefore it appears as a suitable platform for molecular trapping, thereby facilitating SERS detection.[14−17] Furthermore, GO or rGO have been reported to display chemical effects that contribute to SERS enhancement, in a magnitude that depends on the degree of GO chemical reduction.[18] For example, compared with graphene, mildly reduced GO can increase the chemical enhancement by up to 1 order of magnitude for Rhodamine B molecules. Intense efforts have been made by different research groups to employ GO/rGO as supports of Au/Ag nanoparticles, to achieve high SERS efficiency and for a wide variety of applications, such as a selectivity toward aromatic analytes,[16] for study of cellular uptake mechanisms,[19] and as probe for cancer cell diagnostics.[20] In this context, GO/rGO-noble metal composites have been prepared by either direct reduction of metal salts or by

Special Issue: Materials for Theranostics

Received: March 7, 2014
Accepted: May 6, 2014
Published: May 14, 2014

Scheme 1. Schematic Illustration of the Reduced Graphene Oxide-Nanostar (rGO-NS) Nanocomposite for Drug Delivery Probed by SERS

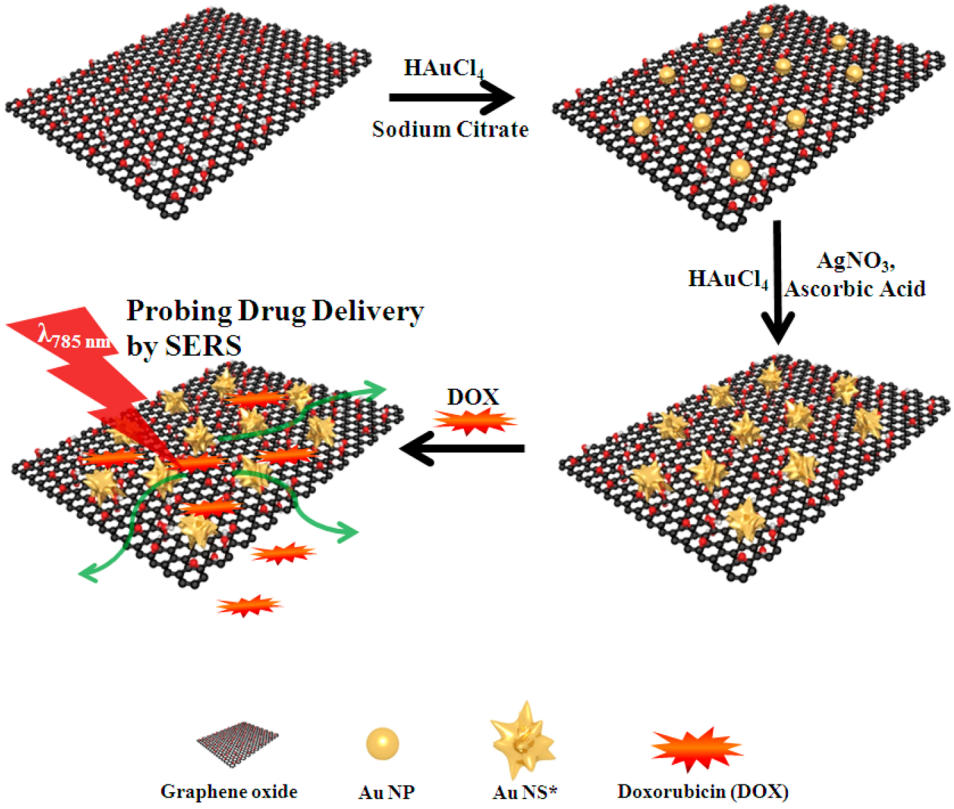

chemical functionalization in the presence of GO.[21−24] Direct reduction yields spherical nanoparticles alone,[21] which are less efficient for SERS applications. Under certain special conditions, direct reduction can produce anisotropic nanostructures, but the control over the final morphology is rather limited.[22] Few attempts have been made toward the preparation of GO-anisotropic NPs composites.[23,24] For instance, in a recent report, Fan et al. reported the preparation of GO-Au nanopopcorn by chemical functionalization, which requires chemical modification of GO by thiol groups.[24]

Regarding important molecules for cancer therapy, doxorubicin (DOX) is an anthracycline antibiotic with a nonthiolated aromatic structure, and it has been used as a drug against a wide range of cancers such as carcinomas, sarcomas and hematological cancers.[25,26] The aromatic structure renders DOX highly hydrophobic, so that its delivery to the target tumors requires loading to a carrier from which it can be subsequently delivered. Recent studies show that the aromatic structure of DOX can actually be exploited to load the drug onto the GO surface via $\pi-\pi$ stacking for *in vitro* and *in vivo* drug delivery or theranostic application.[27−29] Interestingly, the release is pH sensitive and thus it may be accelerated in more acidic tumor microenvironments than in normal tissue.[30]

We herein report the seed-mediated synthesis of gold nanostars (Au NS) supported on reduced graphene oxide (rGO) and the application of such hybrids as an active SERS material for the anticancer drug doxorubicin (DOX) loading and release, as indicated in Scheme 1. Seed-mediated growth is applied as a controllable way to synthesize Au NS on top of the rGO surface, with no need of surfactant or polymer stabilizers. Importantly, the localized surface plasmon resonances of these rGO-Au NS hybrid nanosheets could be tuned within the visible and near-IR (NIR) range, by simply varying growth reaction parameters. Such hybrid structures exhibit improved colloidal stability, enhanced SERS activity over bare Au nanostars, and sensitive SERS response toward aromatic Raman-active molecules. The role of rGO is thus protecting the nanostars from aggregation and bringing the aromatic molecules closer to the nanoparticles surface for efficient SERS. Furthermore, we demonstrate the potential for theranostics through application of SERS to monitor DOX loading and its pH-dependent release from rGO-NS. Such rGO-Au NS composites with abilities to act as SERS active material and interact with aromatic drug molecules show promising potential both as drug delivery carrier and to track the delivery process in biological media.

2. EXPERIMENTAL DETAILS

2.1. Materials. Graphene oxide stock solution (4 mg/mL) was purchased from Graphenea, San Sebastian, Spain. Hydrogen tetrachloroaurate (III) trihydrate ($HAuCl_4 \cdot 3H_2O$, ≥ 99.9%), silver nitrate ($AgNO_3$, ≥ 99.0%), L-ascorbic acid (AA, ≥ 99%), sodium citrate tribasic dihydrate (≥98%), citric acid (≥99.5%), 4-mercaptobenzoic acid (MBA), crystal violet (CV), doxorubicin (DOX), and (3-aminopropyl)triethoxysilane (APTES, ≥ 98%) were all purchased from Sigma-Aldrich. Hydrochloric acid solution (37%), nitric acid (65%) and sulfuric acid (96%) were purchased from Panreac. Hydrogen peroxide (35% w/w, extra pure) was purchased from Scharlau. Microscope glass slides (2947−75 × 25) were from Corning (USA). Milli-Q water (18.2 MΩ cm) was used in all experiments.

2.2. Synthesis of Reduced Graphene Oxide-Au Nanoparticle (rGO-NP) Composites. The rGO-NP nanocomposites were synthesized by a modified literature method.[21] Briefly, graphene oxide aqueous suspension (1 mL, 4 mg/mL) was diluted with 50 mL water and then $HAuCl_4$ solution (80 μL, 158.3 mM) was added and

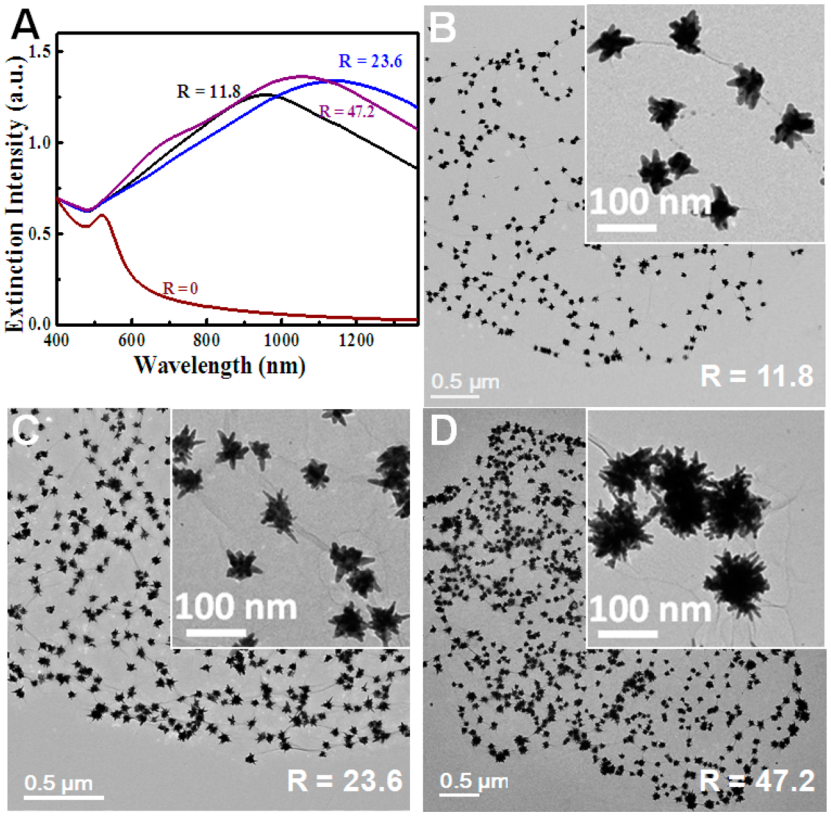

Figure 1. Morphology tuning of rGO-NS through $R = [Au^{3+}]/[Au^0]$. (A) Extinction spectra of rGO-NS synthesized with different R values when using rGO-NP as seeds and $[Ag^+] = 80\ \mu M$. (B–D) TEM images of nanostars formed with R values of (B) 11.8, (C) 23.6, and (D) 47.2.

the mixture was stirred for 30 min. Thereafter, the solution was heated up to ~85 °C, and 500 μL of sodium citrate (1.0 M) was added dropwise. The above reaction mixture was stored for 1 h to form rGO-NP colloidal solution. rGO solution was also prepared following the same procedure without $HAuCl_4$.

2.3. Synthesis of Reduced Graphene Oxide-Au Nanostar (rGO-NS) Composite and Control Samples. The rGO-NS nanocomposites were synthesized by a modified seed-mediated growth method.[7] Briefly, different amounts of the as-prepared rGO-NP seed solution (Au NP, ~15.2 nm average diameter, on rGO surface, see Figure S1 in the Supporting Information for TEM images) were added to 10 mL of a 0.25 mM $HAuCl_4$ solution in a 20 mL glass vial, followed by 5 μL of 1 M HCl at room temperature under moderate stirring. Quickly, different amounts of silver nitrate and 50 μL of ascorbic acid (AA, 100 mM) were added quickly to the above solution. The solution was stirred for 20 s as its color rapidly turned from light red to blue or greenish-black. The morphology of NS was tuned by changing the R value ($R = [Au^{3+}]/[Au^0]$) and $[Ag^+]$ during the synthesis. Control samples including NS (bare Au NP as the seeds with the same $[Au^0]$ and average particle size ~15.2 nm) and NS (rGO as the seeds with the same [rGO]) were synthesized following the same above process except for the use of different seed solutions.

2.4. Colloidal Stability. The colloidal stability of different Au nanoparticles (rGO-NS prepared at different R values and $[Ag^+]$, rGO-NP seed, and bare NS) were studied by UV–visible–near infrared (UV–vis–NIR) spectrometry. Extinction spectra of different Au nanoparticles, both freshly prepared and after 3 days, as well as photographs of the colloidal solutions were recorded.

2.5. Fabrication of rGO-NS or NS Nanostructured Films. Microscope glass slides were cut into small pieces (5 mm × 8 mm) and first cleaned by sequential ultrasonication in acetone, ethanol, and Milli-Q water for 15 min each, which was followed by treatment with (H_2SO_4 (96%)/H_2O_2 (35%)) (3:1 (v/v) solution with a boiling for 30 min). After thoroughly rinsing with Milli-Q water and ethanol, the cleaned glass substrates were dried in air. Second, the clean glass substrates were immersed in a 10% solution of APTES in ethanol for 16 h. The substrates were then rinsed profusely with ethanol to remove unbound APTES from the surface and dried in air. Third, the silane-modified glass substrate was immersed into colloidal rGO-NS, bare NS or rGO-NP seed solution ($[Au^0] \approx 0.268$ mM) for 12 h, resulting in the formation of a particle film on the glass surface. For analyte sensing, the resulted substrates were incubated in 1 mL of CV (1 μM) aqueous solution at room temperature overnight. Subsequently, the substrate was rinsed with water, and gently dried with nitrogen gas. The prepared substrates were wrapped in aluminum foil for further processing.

2.6. Raman Response of rGO, rGO-NP, and rGO-NS Interacting with Aromatic Raman Active Molecules. Aromatic Raman active molecules, which include mercaptobenzoic acid (MBA), crystal violet (CV), and doxorubicin (DOX), were selected to study the Raman response when interacting with rGO or rGO derivatives. MBA (10 μM), CV (5 μM), and DOX (50 μM) were used during Raman measurements under 785 nm laser excitation, whereas rGO or rGO derivatives were all kept at [rGO] ≈ 12 μg/mL.

2.7. Interaction of DOX with rGO-NS and DOX Loading. The interaction of doxorubicin with rGO-NS was studied by fluorescence quenching, UV–vis spectroscopy and Raman scattering. Briefly, an aqueous DOX (10 μM) solution was prepared and monitored by UV–vis and fluorometry, followed by gradual addition of rGO-NS solution aliquots ([rGO] = ~12 μg/mL). Fluorescence spectra were collected after each addition. After the final addition of rGO-NS into DOX solution and incubation, the formed rGO-NS-DOX particles were collected by centrifugation, and the supernatant was measured by UV–vis. A [DOX] calibration curve was prepared to determine the exact concentration of DOX, based on absorption measurements. By comparing the [DOX] difference before and after incubation with rGO-NS, the loading efficiency of DOX onto rGO-NS was calculated. The DOX-loaded rGO-NS and control samples (rGO-NS, and DOX in water) were characterized by UV–vis and Raman scattering

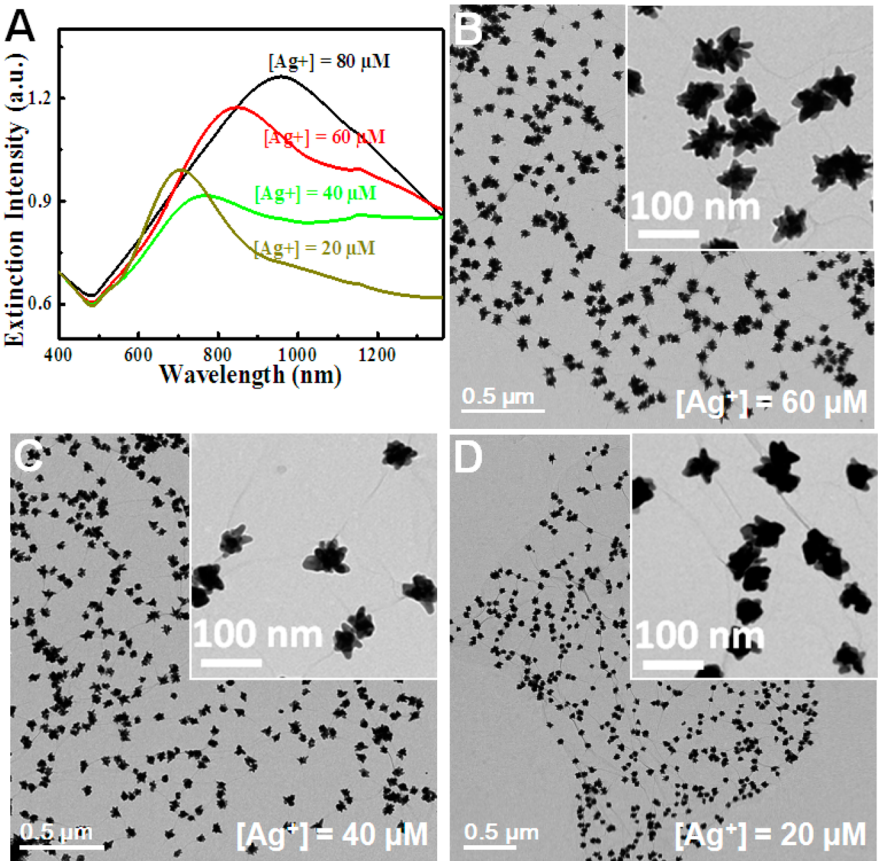

Figure 2. Morphology tuning of rGO-NS through [Ag^+]. (A) Extinction spectra of rGO-NS synthesized with different [Ag^+] when using rGO-NP as seeds, with R = 11.8. (B-D) TEM images of nanostars grown with [Ag^+] of (B) 60, (C) 40, and (D) 20 μM. Note: the small peak in the UV−vis spectra at 1150 nm arises from an instrumental defect.

measurements (785 nm excitation wavelength, exposure 10 s, and accumulation 1 time).

2.8. SERS Study of pH-Dependent DOX Release from rGO-NS. DOX-loaded rGO-NS was prepared by incubating rGO-NS ([rGO] ≈ 12 μg/mL) with DOX ([DOX] ≈ 70 μM) overnight. The DOX loading efficiency was determined to be ∼36% for all samples used for pH-dependent DOX release study (∼1.3 mg of DOX per 1 mg of rGO from rGO-NS). Briefly, the DOX-loaded rGO-NS was dispersed in buffers with different pH values (4.0, 6.0, and 7.4). After incubation for more than 3 h, the rGO-NS-DOX particles were collected by centrifugation, and the supernatant was removed for UV−vis measurements. The remaining rGO-NS-DOX was redispersed in buffers with the same pH values as that before washing. Solution Raman scattering spectra were recorded for all samples with 785 nm excitation laser. Control samples, including rGO-NS background, DOX in water (∼70 μM), and DOX bulk, were also monitored in the same way.

2.9. Instrumentation and Characterization. UV−vis spectroscopy (Agilent UV−visible, ChemStation) was used to collect extinction spectra of colloidal solutions immediately after synthesis. A spectrophotometer (Cary 5000 Varian) was used to collect UV−vis−NIR spectrum of aqueous sample solution. Samples were measured in either 10 mm quartz cuvettes or in 1 mm quartz cuvettes (when specified). A Horiba-Jovin Yvon spectrofluorometer was used to determine photoluminescence spectra with excitation at 490 nm, emission 500−800 nm, and slit 5 nm. Transmission electron microscopy (TEM) images were obtained using JEOL JEM-2010 (120 kV) or JEM-2100F (200 kV) electron microscopes. TEM sampling was done by drop-casting the particle solution on the TEM copper grids and dried in air. Scanning electron microscopy (SEM, JSM-6490LV, 10 kV) was also used to characterize the surface morphologies of the thin films composed of rGO-NS, rGO-NP, and NS. Zeta-potential was measured in a Malvern Zetasizer. X-ray photoelectron spectroscopy (XPS, SPECS SAGE HR100 system, equipped with a 100 mm mean radius PHOIBOS analyzer) was used to study surface elemental composition and chemical state analysis. A Raman-IR microscope (Renishaw InVia Raman spectrometer) was used for both solution and substrate Raman studies: solution Raman was measured after incubation of the Raman tag with the freshly prepared NS or rGO-NS colloids. For each spectrum, the background signal (colloidal sample in the absence of Raman tag) was subtracted. Glass vials (Thermo Scientific, National C4015−96, 1 mL clear sepcap vials, 8 × 40 mm) were used for all solution Raman measurements. Substrate Raman scattering was measured after checking the silicon peak as an internal standard for Raman shift calibration.

3. RESULTS AND DISCUSSION

Our approach to the preparation of rGO-NS composite colloids starts from a graphene oxide aqueous solution as shown in Scheme 1. After introducing $HAuCl_4$ and sodium citrate at ∼85 °C, Au nanoparticles are formed *in situ* on the partially reduced graphene oxide (rGO) surface, with an average size of 15.2 nm (see Figure S1 in the Supporting Information). The prepared rGO-NP was then used as the seed to *in situ* grow NS on the rGO surface, following a modified nanostars synthesis method.[7] The partial reduction of GO was confirmed by UV−vis and XPS analysis (see Figure S2 in the Supporting Information). The disappearance of the band around 300 nm and the absorption increase at the UV−vis region indicate the recovery of the electronic conjugated structure after reduction, in agreement with previous reports.[31] XPS further confirmed

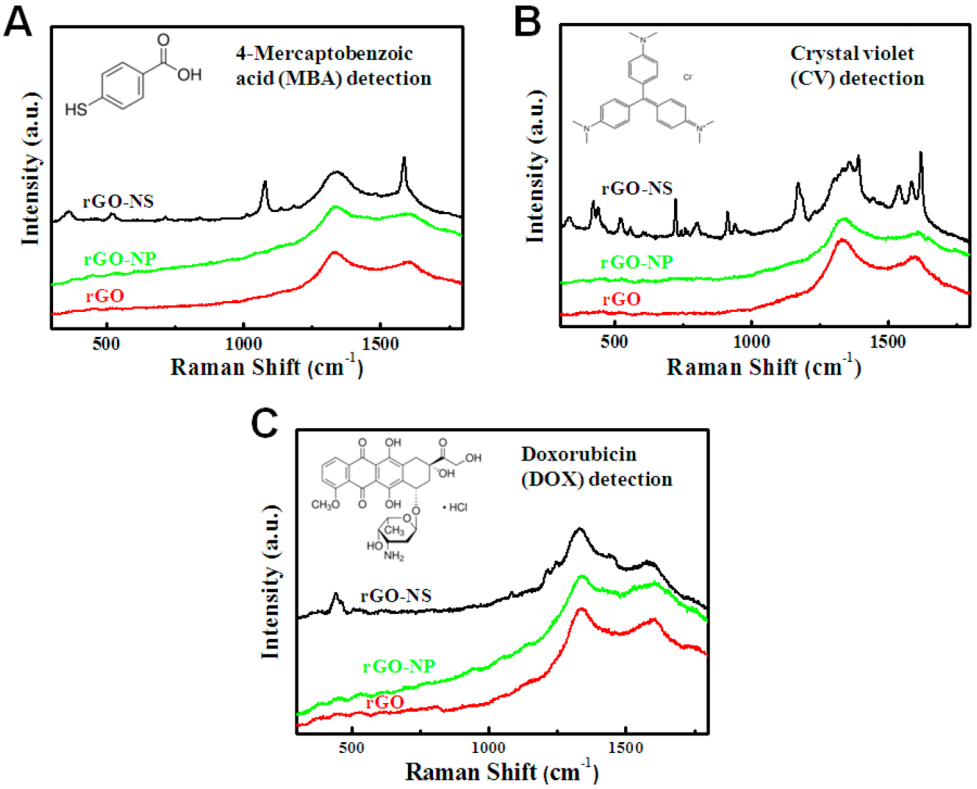

Figure 3. Raman scattering and SERS spectra recorded 785 nm laser excitation for rGO, rGO-NP and rGO-NS interacting with aromatic Raman molecules, including: (A) 4-mercaptobenzoic acid (MBA), (B) crystal violet (CV), and (C) doxorubicin (DOX).

that the C−C/C−O ratio increased after GO reduction (see Figure S2 in the Supporting Information).

Interestingly, the morphology of the NS on rGO could be tuned by different strategies. Figure 1 shows that, by simply changing the molar ratio between gold salt and gold atoms in the seeds, $R = [Au^{3+}]/[Au^0]$, the obtained rGO-NS show different morphologies along with distinct LSPR spectra. As seen in the TEM images, the average NS size varies from 67.3 nm with 9 branches (on average) for $R = 11.8$, to 73.4 nm with 11 branches for $R = 23.6$, and 117.7 nm with 23 branches for $R = 47.2$. Correspondingly, the LSPR spectra show red-shifted LSPR bands when the R value is increased from 11.8 to 23.6. Further increasing R to 47.2 leads to a broader spectrum with a shoulder around 700 nm. When no gold nanoparticles were present as seeds during the synthesis ($R = \infty$), an LSPR band near 750 nm was observed with higher intensity, which can be considered as a spectral feature for growth without seed-mediated control (see Figure S3 in the Supporting Information). In general, all formed Au NS are specifically confined on the rGO surface with wrinkles clearly visible under low magnification TEM imaging. These wrinkles or folded rGO sheets are more apparent for larger NS grown from rGO-NP, and probably affected by sample drying on the TEM grid.

The R-dependent trend of the LSPR bands for rGO-NS is similar to that previously reported for the seeded growth of Au NS in PVP/DMF mixtures,[32] in both cases featuring a tunable spectrum profile by varying R value. As a control experiment, the seed-mediated Au NS synthesis in the absence of rGO was also conducted under similar conditions.[7] We found that, in contrast to NS grown on rGO-NP with similar seed size (15.2 nm average diameter) (Figure 1B), NS grown from Au NP seeds display narrower and blue-shifted LSPR spectra (see Figure S3A in the Supporting Information), along with thinner and more abundant branches (see Figure S3B in the Supporting Information). Although in principle one would expect that thinner branches should lead to red-shifted LSPR,[7] the organization of the NS on the rGO nanosheets surface, plasmon coupling and refractive index effects may originate the experimentally observed LSPR band red-shift and broadening. When using plain rGO (no Au) as seed, the formed particles show broader LSPR spectra and polydispersity (see Figure S3A, C in the Supporting Information), together with dendritic morphologies, similar to a previous report.[33] Such dendritic NS resemble the small fraction of larger NS obtained when using rGO-NP as seeds (Figure 1), and may be ascribed to rGO defects and functional groups acting as the nucleation sites.[33,34]

The morphology of Au NS confined on the rGO surface could also be tuned by simply varying $[Ag^+]$, while keeping all other parameters constant during NS growth. As shown in Figure 2, when $[Ag^+]$ is increased from 20 to 80 μM, the obtained rGO-NS show larger overall size and more branches (58.8 nm with 6 branches for $[Ag^+] = 20$ μM; 61.4 nm with 8 branches for $[Ag^+] = 40$ μM; 66.4 nm with 9 branches for $[Ag^+] = 60$ μM; and 67.3 nm with 9 branches for $[Ag^+] = 80$ μM), along with red-shifted LSPR spectra from ~700 nm for $[Ag^+] = 20$ μM, to ~1000 nm for $[Ag^+] = 80$ μM. The silver concentration-dependent trend of the rGO-NS LSPR band is similar to that previously reported for Au NS synthesis in the absence of rGO,[7] both with tunable spectrum profile by varying $[Ag^+]$. However, the required $[Ag^+]$ was found to be higher in the presence of rGO in order to obtain similar morphologies as those grown from bare NP (see Figure S4 in the Supporting Information), which seems to indicate that silver ions not only interact with the Au NP seeds during growth but can also be

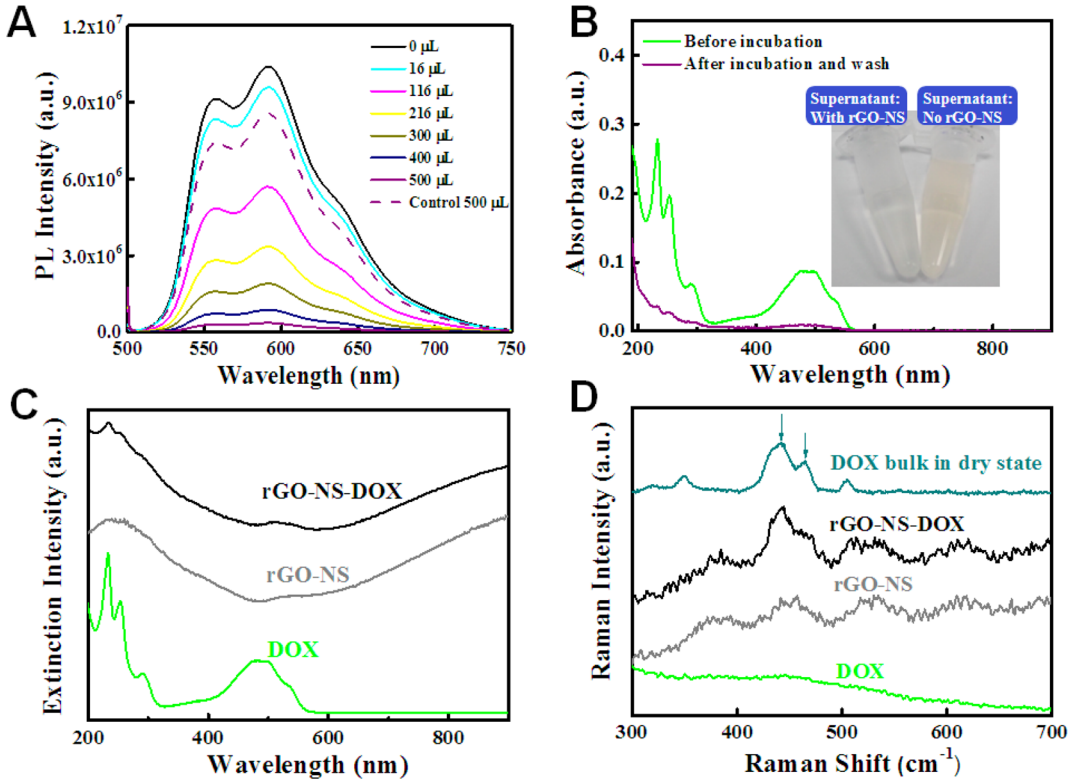

Figure 4. Interaction of DOX with rGO-NS and its DOX loading: (A) Quenching of DOX fluorescence upon addition of rGO-NS (up to 500 μL, 12 μg/mL [rGO]) into 10 μM DOX solution, together with the control sample diluted with 500 μL of pure water. (B) UV–vis spectra of the supernatant after spinning down rGO-NS upon incubation with DOX; the inset shows a photograph of the supernatants. (C) UV–vis spectra of rGO-NS-DOX, rGO-NS and DOX solutions. (D) Raman scattering spectra of rGO-NS-DOX, rGO-NS, and DOX solutions. The spectrum for bulk DOX in the dry state is also provided to indicate the positions of DOX Raman scattering bands (arrows indicate the strongest DOX Raman bands).

adsorbed on rGO. As a consequence, the transformation of Au NP into NS on rGO surface is significantly different to that occurring in the absence of rGO, though both share general synthetic strategies such as morphology control by tuning reaction parameters.

An immediate advantage of using rGO as a substrate for NS growth is that it provides enhanced colloidal stability with no need of additional surfactant or polymer, thereby maintaining an accessible metal surface. Bare NS easily aggregate in the absence of capping molecules such as sodium dodecylsulfate (SDS) or thiolated poly(ethylene glycol) (PEG),[7,8] mainly due to van der Waals attraction and poor double layer repulsion. Figure S5 in the Supporting Information illustrates the significantly higher stability of rGO-NS as compared to bare NS. After 3 days, rGO-NS (R = 11.8, [Ag^+] = 80 μM) retain 90% of the initial LSPR absorbance, with negligible changes in the spectral profile. In contrast, bare NS are found to separate from solution, either by adsorption on the vial walls or through aggregation and precipitation, with less than 10% absorbance retained and blue-shifted LSPR band. The colloidal stability of rGO-NS however is hindered when higher R values are used, as shown in the UV–vis–NIR spectra in Figure S5 in the Supporting Information (Note that 90% intensity is retained for R = 11.8, whereas 70% only for R = 23.6, 40% for R = 47.2, and 10% for bare NS). For completeness, rGO-NS prepared at different [Ag^+], as well as rGO-NP seed, were also compared (see Figure S6 in the Supporting Information). The difference in colloidal stability can be readily estimated from the digital photographs. On the basis of the above results, the most stable rGO-NS (R = 11.8), which show a zeta-potential of −40 mV (see Figure S7 in the Supporting Information), was selected to further study its interaction with Raman active molecules.

The Raman scattering and SERS activity of several molecules was studied in the presence of rGO-NS, as well as rGO and rGO-NP seeds. Three different aromatic Raman molecules, namely 4-mercaptobenzoic acid (MBA), crystal violet (CV), and doxorubicin (DOX), were selected (see molecular structures in Figure 3). At the same concentration, molecules in the presence of rGO and rGO-NP do not produce any characteristic Raman scattering signal, whereas the use of rGO-NS clearly allows to identify the SERS signals of MBA, CV, and DOX. Considering the similar [rGO] in rGO, rGO-NP, and rGO-NS samples, the different Raman response may be attributed to strong electromagnetic enhancement (EM) and nanoantena effect,[35,36] the strongest for rGO-NS, lower for rGO-NP, and no EM for plain rGO. In addition, substrate Raman test (see Experimental Details) using CV as probe shows the strongest SERS intensity for rGO-NS over either bare Au NS or rGO-NP seed (see Figure S8 in the Supporting Information). These results clearly demonstrate that the Raman enhancing performance of rGO-supported Au NS shows a significant improvement when compared with that obtained without rGO support.

Considering the importance of the polyaromatic drug molecule DOX for cancer therapy, we explored the use of SERS to monitor DOX loading and release, using the developed rGO-NS as an active SERS material. The interaction between rGO-NS and DOX was first confirmed by fluorescence quenching experiments as shown in Figure 4A. Upon addition of rGO-NS to a DOX aqueous solution (10 μM), DOX

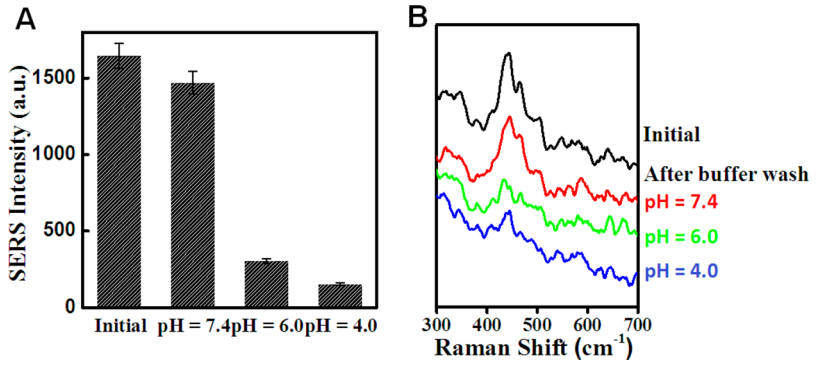

Figure 5. SERS study on pH-dependent DOX release from rGO-NS: (A) SERS intensity at 443 cm^{-1} for rGO-NS-DOX after incubation and wash with different buffers (pH 4, 6, and 7.4). (B) SERS spectra registered for the same samples, after background subtraction.

fluorescence dramatically decreased, e.g., 90% decrease in fluorescence intensity when 500 μL rGO-NS (final [rGO] = 4 μg/mL) was added, whereas the same volume of water leads to a minor variation of PL intensity (dilution effect consideration, see Figure S9 in the Supporting Information). After centrifugation of the above solution (incubating DOX with rGO-NS), the supernatant was found to be colorless, in contrast to a yellow color of DOX solution in the absence of rGO-NS (Figure 4B). Calculation of DOX concentration using a linear fitting calibration curve (absorbance@485 nm vs [DOX], see Figure S10 in the Supporting Information) shows that 88% of the drug was loaded onto the rGO-NS surface. The UV−vis spectrum of rGO-NS-DOX after washing shows clear combined peaks from DOX and rGO-NS. When excited under the 785 nm laser, rGO-NS-DOX solution displays SERS bands that are characteristic for DOX, such as deformational modes in plane bending (C−O at 443 cm^{-1} and C═O at 465 cm^{-1}),[37] in similar positions to those from a DOX dry film (Figure 4D). In contrast, control samples (either rGO-NS only or DOX in water) yield no DOX characteristic Raman bands. The above results clearly demonstrate that DOX was efficiently loaded onto rGO-NS.

Finally, we studied by SERS the DOX release from rGO-NS at different pH values. Equal amounts of DOX-loaded rGO-NS (DOX loading efficiency ∼36% for all samples, or ∼1.3 mg DOX per mg of rGO in rGO-NS, see Figure S11A in the Supporting Information) were dispersed in buffers with different pH values, including citric acid-sodium citrate buffers (pH 4.0 buffer with 0.1 M ionic strength, and pH 6.0 buffer with 0.1 M ionic strength), and phosphate buffer (pH 7.4 buffer with 0.1 M ionic strength). After incubation for 3 h, the rGO-NS-DOX particle solutions were collected by centrifugation, and the supernatant was removed for UV−vis spectroscopy measurements. The remaining rGO-NS-DOX was redispersed in buffers with the same pH values as those before washing. Solution SERS shows that ca. 90% of the DOX SERS signal is maintained at pH 7.4, whereas only 9 and 18% are retained for pH 4.0 and 6.0, respectively (see Figure 5 and Figure S11B in the Supporting Information). Interestingly, the UV−vis spectra of the obtained supernatants after incubation in different pH buffers show varying DOX absorbance intensity, the highest value obtained for pH 4.0 and the lowest for pH 7.4 (see Figure S11C in the Supporting Information), which is in agreement with the SERS response from different pH buffer-washed samples. The observed favored DOX release from rGO-NS under acidic conditions can be ascribed to the pH-dependent $\pi-\pi$ stacking interaction between DOX and the aromatic domains of rGO. Ionization of the amino groups in DOX molecules increases at lower pH values, in turn leading to an increase in DOX solubility and detachment from the rGO-NS surface.[27−29] Therefore, we can conclude that the composite substrates used here can be applied to capture and release DOX, and both processes can be monitored by SERS.

4. CONCLUSIONS

In summary, we have developed colloidal composites comprising gold nanostars supported on reduced-graphene oxide (rGO-NS) as an active SERS material for anticancer DOX loading and pH-dependent release. Seed-mediated growth was successfully employed to grow Au NS on the rGO surface in a controllable way, with no need for surfactant or polymer stabilizers. Importantly, the as-developed hybrid nanosheets feature tunable LSPR bands up to the NIR region, by simply tuning R and [Ag^+], improved colloidal stability as compared to bare Au nanostars, and highly sensitive SERS response for aromatic Raman molecules. Furthermore, the use of SERS to monitor the anticancer drug molecule (DOX) loading and pH sensitive release from the rGO-NS support was demonstrated. Such developed rGO-NS nanocomposites show great potential as active SERS materials for SERS-based applications, such as drug delivery and chemotherapy.

■ ASSOCIATED CONTENT

Ⓢ Supporting Information

TEM images and photograph of rGO-NP seeds; UV−vis and XPS analysis of samples including GO, rGO, and rGO-NP; comparison of NS formation among different seeds; effect of [Ag^+] on the synthesis of Au NS; colloidal stability analysis; characterization of rGO-NS for Raman studies; substrate Raman and SERS data; fluorescence monitoring of DOX dilution; UV−vis spectra of DOX at different concentrations; SERS study on pH-dependent DOX release. This material is available free of charge via the Internet at http://pubs.acs.org.

■ AUTHOR INFORMATION

Corresponding Author

*E-mail: llizmarzan@cicbiomagune.es.

Notes

The authors declare no competing financial interest.

■ ACKNOWLEDGMENTS

This work was funded by the European Commission (Grant 310445-2 SAVVY) and the European Research Council (ERC

Advanced Grant 267867 Plasmaquo). The authors thank Dr. Luis Yate for performing XPS measurements.

REFERENCES

(1) Nie, S.; Emory, S. R. Probing Single Molecules and Single Nanoparticles by Surface-Enhanced Raman Scattering. *Science* **1997**, *275*, 1102−1106.

(2) Kneipp, K.; Wang, Y.; Kneipp, H.; Perelman, L. T.; Itzkan, I.; Dasari, R. R.; Feld, M. S. Single Molecule Detection Using Surface-Enhanced Raman Scattering (SERS). *Phys. Rev. Lett.* **1997**, *78*, 1667−1670.

(3) Alvarez-Puebla, R. A.; Liz-Marzán, L. M. Traps and Cages for Universal SERS Detection. *Chem. Soc. Rev.* **2012**, *41*, 43−51.

(4) Rodríguez-Lorenzo, L.; Álvarez-Puebla, R. A.; Pastoriza-Santos, I.; Mazzucco, S.; Stéphan, O.; Kociak, M.; Liz-Marzán, L. M.; García de Abajo, F. J. G. Zeptomol Detection through Controlled Ultrasensitive Surface-Enhanced Raman Scattering. *J. Am. Chem. Soc.* **2009**, *131*, 4616−4618.

(5) Rodríguez-Lorenzo, L.; Álvarez-Puebla, R. A.; García de Abajo, F. J. G.; Liz-Marzán, L. M. Surface Enhanced Raman Scattering Using Star-Shaped Gold Colloidal Nanoparticles. *J. Phys. Chem. C* **2010**, *114*, 7336−7340.

(6) Alvarez-Puebla, R.; Liz-Marzán, L. M.; García de Abajo, F. J. Light Concentration at the Nanometer Scale. *J. Phys. Chem. Lett.* . **2010**, *1*, 2428−2434.

(7) Yuan, H.; Khoury, C. G.; Hwang, H.; Wilson, C. M.; Grant, G. A.; Vo-Dinh, T. Gold Nanostars: Surfactant-Free Synthesis, 3D Modelling, and Two-Photon Photoluminescence Imaging. *Nanotechnology* **2012**, *23*, 075102(1−9).

(8) Yuan, H.; Liu, Y.; Fales, A. M.; Li, Y. L.; Liu, J.; Vo-Dinh, T. Quantitative Surface-Enhanced Resonant Raman Scattering Multiplexing of Biocompatible Gold Nanostars for In Vitro and Ex Vivo Detection. *Anal. Chem.* **2013**, *85*, 208−212.

(9) Stiles, P. L.; Dieringer, J. A.; Shah, N. C.; Van Duyne, R. P. Surface-Enhanced Raman Spectroscopy. *Annu. Rev. Anal. Chem.* **2008**, *1*, 601−626.

(10) Álvarez-Puebla, R. A.; Contreras-Cáceres, R.; Pastoriza-Santos, I.; Pérez-Juste, J.; Liz-Marzán, L. M. Au@pNIPAM Colloids as Molecular Traps for Surface-Enhanced, Spectroscopic, Ultra-Sensitive Analysis. *Angew. Chem., Int. Ed.* **2009**, *48*, 138−143.

(11) Contreras-Cáceres, R.; Abalde-Cela, S.; Guardia-Girós, P.; Fernández-Barbero, A.; Pérez-Juste, J.; Alvarez-Puebla, R. A.; Liz-Marzán, L. M. Multifunctional Microgel Magnetic/Optical Traps for SERS Ultradetection. *Langmuir* **2011**, *27*, 4520−4525.

(12) Doering, W. E.; Nie, S. Spectroscopic Tags Using Dye-Embedded Nanoparticles and Surface-Enhanced Raman Scattering. *Anal. Chem.* **2003**, *75*, 6171−6176.

(13) Ip, S.; MacLaughlin, C. M.; Gunari, N.; Walker, G. C. Phospholipid Membrane Encapsulation of Nanoparticles for Surface-Enhanced Raman Scattering. *Langmuir* **2011**, *27*, 7024−7033.

(14) Huang, X.; Qi, X.; Boey, F.; Zhang, H. Graphene-Based Composites. *Chem. Soc. Rev.* **2012**, *41*, 666−686.

(15) Xu, W.; Mao, N.; Zhang, J. Graphene: a Platform for Surface-Enhanced Raman Spectroscopy. *Small* **2013**, *9*, 1206−1224.

(16) Liu, X.; Cao, L.; Song, W.; Ai, K.; Lu, L. Functionalizing Metal Nanostructured Film with Graphene Oxide for Ultrasensitive Detection of Aromatic Molecules by Surface-Enhanced Raman Spectroscopy. *ACS Appl. Mater. Interfaces* **2011**, *3*, 2944−2952.

(17) Polavarapu, L.; Liz-Marzán, L. M. Towards Low-Cost Flexible Substrates for Nanoplasmonic Sensing. *Phys. Chem. Chem. Phys.* **2013**, *15*, 5288−5300.

(18) Yu, X.; Cai, H.; Zhang, W.; Li, X.; Pan, N.; Luo, Y.; Wang, X.; Hou, J. G. Tuning Chemical Enhancement of SERS by Controlling the Chemical Reduction of Graphene Oxide Nanosheets. *ACS Nano* **2011**, *5*, 952−958.

(19) Huang, J.; Zong, C.; Shen, H.; Liu, M.; Chen, B.; Ren, B.; Zhang, Z. Mechanism of Cellular Uptake of Graphene Oxide Studied by Surface-Enhanced Raman Spectroscopy. *Small* **2012**, *8*, 2577−2584.

(20) Hu, C.; Liu, Y.; Qin, J.; Nie, G.; Lei, B.; Xiao, Y.; Zheng, M.; Rong, J. Fabrication of Reduced Graphene Oxide and Sliver Nanoparticle Hybrids for Raman Detection of Absorbed Folic Acid: a Potential Cancer Diagnostic Probe. *ACS Appl. Mater. Interfaces* **2013**, *5*, 4760−4768.

(21) Goncalves, G.; Marques, P. A. A. P.; Granadeiro, C. M.; Nogueira, H. I. S.; Singh, M. K.; Grácio, J. Surface Modification of Graphene Nanosheets with Gold Nanoparticles: the Role of Oxygen Moieties at Graphene Surface on Gold Nucleation and Growth. *Chem. Mater.* **2009**, *21*, 4796−4802.

(22) Nergiz, S. Z.; Gandra, N.; Singamaneni, S. Self-Assembled High Aspect Ratio Gold Nanostar/Graphene Oxide Hybrid Nanorolls. *Carbon* **2014**, *66*, 585−591.

(23) Kim, Y. K.; Na, H. K.; Lee, Y. W.; Jang, H.; Han, S. W.; Min, D. H. The Direct Growth of Gold Rods on Graphene Thin Films. *Chem. Commun.* **2010**, *46*, 3185−3187.

(24) Fan, Z.; Kanchanapally, R.; Ray, P. C. Hybrid Graphene Oxide Based Ultrasensitive SERS Probe for Label-Free Biosensing. *J. Phys. Chem. Lett.* . **2013**, *4*, 3813−3818.

(25) Weiss, R. B. The Anthracyclines: Will We Ever Find a Better Doxorubicin? *Semin. Oncol.* **1992**, *19*, 670−686.

(26) Carvalho, C.; Santos, R. X.; Cardoso, S.; Correia, S.; Oliveira, P. J.; Santos, M. S.; Moreira, P. I. Doxorubicin: the Good, the Bad and the Ugly Effect. *Curr. Med. Chem.* **2009**, *16*, 3267−3285.

(27) Balcioglu, M.; Rana, M.; Yigit, M. V. Doxorubicin Loading on Graphene Oxide, Iron Oxide and Gold Nanoparticle Hybrid. *J. Mater. Chem. B* **2013**, *1*, 6187−6193.

(28) Wang, F.; Liu, B.; Ip, A. C. F.; Liu, J. Orthogonal Adsorption onto Nano-Graphene Oxide Using Different Intermolecular Forces for Multiplexed Delivery. *Adv. Mater.* **2013**, *25*, 4087−4092.

(29) Huang, J.; Zong, C.; Shen, H.; Cao, Y.; Ren, B.; Zhang, Z. Tracking the Intracellular Drug Release from Graphene Oxide Using Surface-Enhanced Raman Spectroscopy. *Nanoscale* **2013**, *5*, 10591−10598.

(30) Tannock, I. F.; Rotin, D. Acid pH in Tumors and its Potential for Therpeutic Exploitation. *Cancer Res.* **1989**, *49*, 4373−4384.

(31) Iliut, M.; Leordean, C.; Canpean, V.; Teodorescu, C. M.; Astilean, S. A New Green, Ascorbic Acid-Assisted Method for Versatile Synthesis of Au-Graphene Hybrids as Efficient Surface-Enhanced Raman Scattering Platforms. *J. Mater. Chem. C* **2013**, *1*, 4094−4104.

(32) Barbosa, S.; Agrawal, A.; Rodríguez-Lorenzo, L.; Pastoriza-Santos, I.; Alvarez-Puebla, R. A.; Kornowski, A.; Weller, H.; Liz-Marzán, L. M. Tuning Size and Sensing Properties in Colloidal Gold Nanostars. *Langmuir* **2010**, *26*, 14943−14950.

(33) Jasuja, K.; Berry, V. Implantation and Growth of Dendritic Gold Nanostructures on Graphene Derivatives: Electrical Property Tailoring and Raman Enhancement. *ACS Nano* **2009**, *3*, 2358−2366.

(34) Zhou, X.; Huang, X.; Qi, X.; Wu, S.; Xue, C.; Boey, F. Y. C.; Yan, Q.; Chen, P.; Zhang, H. In Situ Synthesis of Metal Nanoparticles on Single-Layer Graphene Oxide and Reduced Graphene Oxide Surfaces. *J. Phys. Chem. C* **2009**, *113*, 10842−10846.

(35) Alvarez-Puebla, R. A.; Agarwal, A.; Manna, P.; Khanal, B. P.; Aldeanueva-Potel, P.; Carbó-Argibay, E.; Pazos-Pérez, N.; Vigderman, L.; Zubarev, E. R.; Kotov, N. A.; Liz-Marzán, L. M. Gold Nanorods 3D-Supercrystals as Surface Enhanced Raman Scattering Spectroscopy Substrates for the Rapid Detection of Scrambled Prions. *Proc. Natl. Acad. Sci. U.S.A.* **2011**, *108*, 8157−8161.

(36) Alvarez-Puebla, R. A.; Zubarev, E. R.; Kotov, N. A.; Liz-Marzán, L. M. Self-Assembled Nanorod Supercrystals for Ultrasensitive SERS Diagnostics. *Nano Today* **2012**, *7*, 6−9.

(37) Gautier, J.; Munnier, E.; Douziech-Eyrolles, L.; Paillard, A.; Dubois, P.; Chourpa, I. SERS Spectroscopic Approach to Study Doxorubicin Complexes with Fe^{2+} Ions and Drug Release from SPION-Based Nanocarriers. *Analyst* **2013**, *138*, 7354−7361.